

Article

Method for Intensive Gas–Liquid Dispersion in a Stirred Tank

Nikolai A. Voinov, Alexander S. Frolov, Anastasiya V. Bogatkova, Denis A. Zemtsov  and Olga P. Zhukova

Institute of Chemical Technology, Reshetnev Siberian State University of Science and Technology,
31 Krasnoyarsky Rabochoy Av., Krasnoyarsk 660037, Russia

* Correspondence: denis_zemtsov.92@mail.ru

Abstract: This article presents the results of hydrodynamics and mass exchange in a stirred tank upon the introduction of gas from an open gas vortex cavity into local liquid regions with reduced pressure. It establishes conditions for the intensive dispersion of gas. Velocity fields and liquid pressure behind the stirrer paddles are determined by numerical simulation in OpenFOAM. The gas content value, gas bubble diameters, and phase surface are determined experimentally. The stirrer power criterion is calculated by taking into account the gas content and power input. The experimental mass transfer data based on the absorption of atmospheric oxygen into water during the dispersion of gas from the open vortex cavity in the local liquid regions behind the rotating stirrer paddles are presented. In this case, the energy dissipation from the rotating stirrer reaches 25 W/kg, with a phase surface of 1000 m⁻¹ and a surface mass transfer coefficient of up to 0.3·10⁻³ m/s. These parameters are obviously higher than the data obtained in the apparatus for mass exchange through surface vorticity. The advantage of the given method for gas dispersion in a liquid is the functional stability of the apparatus regardless of how deep the stirrer is immersed in the liquid or the temperature or pressure of the gas. Apparatuses based on the intensive gas dispersion method allow for varying the mass transfer coefficient and gas content across a broad range of values. This allows establishing a dependency between the experimentally obtained mass transfer coefficient, energy dissipation, and phase surface values. An equation for calculating the mass transfer coefficient is formulated by taking into account the geometric parameters of the stirrer apparatus based on the stirring power and phase surface values.



check for updates

Citation: Voinov, N.A.; Frolov, A.S.; Bogatkova, A.V.; Zemtsov, D.A.; Zhukova, O.P. Method for Intensive Gas–Liquid Dispersion in a Stirred Tank. *ChemEngineering* **2023**, *7*, 30. <https://doi.org/10.3390/chemengineering7020030>

Academic Editors: Thomas Grützner and Bernhard Seyfang

Received: 14 February 2023

Revised: 30 March 2023

Accepted: 31 March 2023

Published: 4 April 2023



Copyright: © 2023 by the authors. Licensee MDPI, Basel, Switzerland. This article is an open access article distributed under the terms and conditions of the Creative Commons Attribution (CC BY) license (<https://creativecommons.org/licenses/by/4.0/>).

Keywords: energy dissipation; gas content; gas vortex; mass transfer coefficient; mass transfer; numerical simulation; paddle stirrer; phase interface; stirring power

1. Introduction

Gas–liquid stirred tanks find wide application in the biotechnology, chemical, food, pharmaceutical, and petrochemical industries. They are used as bioreactors in the cultivation of bacteria, aeration tanks in wastewater treatment, flotation units for ore separation, as well as hydrogenation, chlorination, and alkylation reactors [1–9].

Stirred tanks equipped with bubble columns for dispersing gas into the liquid have found the widest application [10] (Figure 1a). Further improvements in stirred tanks have led to the development of apparatuses with a gas-phase supply into the liquid through surface vortices (Figure 1b) [6,11–14], with gas ejection into the liquid using various units (Figure 1c) in particular by installing a circulating tube [6,15–17], as well as with gas supply into the liquid through a hollow shaft (Figure 1d) [6,7,14,18–21].

The tanks described above do not require gas transportation units and provide a flow circuit without needing significant capital and operating expenses.

When gas is supplied to the liquid through surface vortices (see Figure 1b), a low rotational speed of 300–700 rpm is maintained in the stirred tank to keep the liquid on the surface of the stirrer paddles. This ensures a low gas content not exceeding 0.1 and a low mass transfer coefficient reaching 0.1 s⁻¹. As the rotational speed of the stirred tank

increases, the liquid is squeezed out by centrifugal force from the paddle surface, and the gas dispersion either decreases or stops completely.

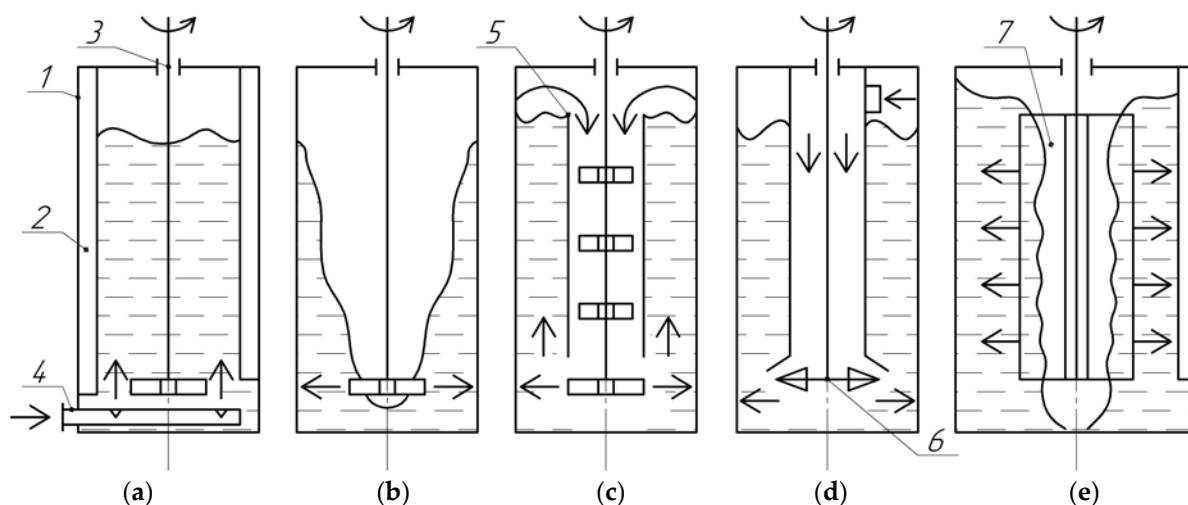


Figure 1. Different methods for dispersing gas into a liquid in a stirrer apparatus: 1—housing; 2—partition; 3—shaft; 4—bubbler; 5—circulation tube; 6—self-priming stirrer; 7—stirrer paddle; gas supply through (a–e): (a) bubbler; (b) surface vortices; (c) circulation circuit; (d) self-priming stirrer; (e) low pressure zones behind the paddle.

Installing circulating tubes with stirrers in the tank complicates the tank design and requires more stirring power.

In tanks with self-priming stirrers, a reduced pressure is provided at the stirrer mounting site that contributes to moving the gas into the liquid by forming an effective phase interface. The disadvantage of such units is that their operation depends on the liquid column height in the tank, the rotational speed, and the gas operating pressure. Stirrers are difficult to manufacture and have a relatively large diameter for greater stirring power.

Of the above schematic diagrams of gas–liquid dispersion, the one with the gas phase supply into the liquid through surface vortices is structurally the simplest.

We assumed that gas dispersion from the gas vortex cavity into the liquid is caused by the appearance of reduced pressure regions in the liquid located directly behind the rotating paddles of the stirrer. The pressure drop causes the gas to move into these regions and be subsequently released into the tank space. Proceeding from this, a design concept was set up (see Figure 1e) that consists of making the shaft paddle equal to the liquid column height in the tank, as well as installing removable or movable partitions on the tank wall, which ensures the adjustment of parameters of the gas vortex cavity and keeps liquid on the paddle surfaces. This allowed for providing local regions with reduced pressure throughout the paddle height and ensuring intensive gas dispersion. Thus, an increase in the phase interface and energy dissipation was ensured, with intensification of the entire mass transfer process. To date, despite the variety of methods for gas–liquid dispersion from a vortex cavity, the conditions ensuring an intensive transition of gas into a liquid have not been sufficiently studied. A better understanding of this phenomenon will help improve this type of tank and increase its efficiency.

The objective of this work is to determine the stirrer process and design parameters under which intensive gas–liquid dispersion from a gas vortex cavity is carried out, and to study hydrodynamics and mass transfer in a tank.

Numerical simulation in OpenFOAM is used to determine the velocity fields and liquid pressures in the stirrer. OpenFOAM is an interactive environment that is based on the control volume approach [22,23].

This approach is the most versatile for describing the hydrodynamic problem in this study. A similar research method was described in [24].

The software uses a generalized version of the Navier–Stokes equations for calculating the hydrodynamic parameters of the moving stream as follows:

$$\left\{ \begin{array}{l} \frac{\partial u_i}{\partial x_i} = 0 \\ \rho_L \frac{\partial u_i}{\partial T} + \rho_L \cdot u_j \frac{\partial u_i}{\partial x_j} = -\frac{\partial P}{\partial x_i} + \frac{\partial}{\partial x_j} \cdot \left(\mu \frac{\partial u_i}{\partial x_j} \right) \end{array} \right\}, \quad (1)$$

where u_i and u_j are the velocity vector components ($i, j = 1, 2, 3$), P is the pressure (Pa), ρ_L is the liquid density (kg/m^3), μ is the medium dynamic viscosity coefficient ($\text{Pa} \cdot \text{s}$), x_i and x_j are coordinates, and T is the time (s).

To determine the mass exchange properties of the dispersion method developed and studied in the paper [25], known hydrodynamic and mass exchange data were analyzed.

As numerous studies have shown, the gas content in a stirred tank during bubbling (schematic diagram in Figure 1a) depends on the stirrer type, tank diameter, physical parameters of the liquid, rotational speed, and gas flow, and is 0.02–0.28 [6,7,26–35].

The gas content in the tank when the gas is supplied through a hollow vortex (schematic diagram in Figure 1b [7]), circulating tubes (Figure 1c [6,16]), or the self-priming stirrer (Figure 1d [7]), is at most 0.1.

Therefore, determining the phase surface required knowing the gas content in the stirrer apparatus under the intensive dispersion method.

The influence of different stirrer parameters on energy consumption has been demonstrated in numerous studies, for example [28,36]. The presence of the gas phase in the liquid during stirring leads to a decrease in energy consumption compared to the results for a single-phase flow [27,28,37,38].

Due to the absence of any reliable power calculation methods or experimental data, stirrer behavior during intensive gas dispersion continued to be studied.

Numerous works have been devoted to studying mass transfer in a stirred tank when gas is supplied through a bubble condenser (Figure 1a). It is known that the value of the mass transfer coefficient depends both on the energy dissipation and on the gas bubble diameter [7,15,18,38–40].

For example, the dependency for calculating the mass transfer coefficient in a stirrer apparatus is as follows [10]:

$$Sh = 0.33 \cdot \left(\frac{n \cdot d_s \cdot d_b}{\nu} \right)^{0.6} \cdot Sc^{0.5}, \quad (2)$$

where Sh is the Sherwood criterion (–), n is the rotational speed (s^{-1}), d_s is the stirrer diameter (m), d_b is the bubble diameter (m), ν is the kinematic viscosity of the fluid (m^2/s), and Sc is the Schmidt criterion (–).

Or, as follows [41]:

$$\frac{\beta \cdot d_s^2}{D_l} = 0.95 \cdot \left(\frac{n \cdot d_s^2}{\nu} \right)^{1.55} \cdot Sc^{0.5} \cdot \left(\frac{\rho_L \cdot \nu^2}{\sigma \cdot d_s} \right)^{0.6} \cdot \left(\frac{s}{d_s} \right)^{1.07}, \quad (3)$$

Where β is the mass transfer coefficient (s^{-1}), D_l is the oxygen diffusion coefficient in water at operating temperature (m^2/s), σ is the surface tension coefficient (N/m), and s is the stirrer pitch (m).

However, these equations work satisfactorily only under the conditions they were produced.

The most promising equations for practical application are ones that are based on energy dissipation taking into account the influence of the structural parameters of the stirring unit [42].

This leads to the following dependency [10]:

$$\beta = 3 \cdot 10^4 \cdot \varepsilon^{0.64} \cdot u_g^{0.6} \cdot D_l^{0.5}, \quad (4)$$

where ε is the energy dissipation (W/kg) and u_g is the gas velocity (m/s).

Or, as follows [43]:

$$\beta = 112 \cdot \varepsilon^{0.44} \cdot \varphi^{0.67}, \quad (5)$$

where φ is the gas content (-).

There are other similar dependencies [44].

The equations above have a significant error, since they do not account for the influence of the phase surface on the mass exchange.

This study establishes the relation between the max transfer intensity, energy dissipation, and phase surface.

2. Materials and Methods

Figure 2 presents a schematic diagram of the stirred tank for studying intensive gas–liquid dispersion.

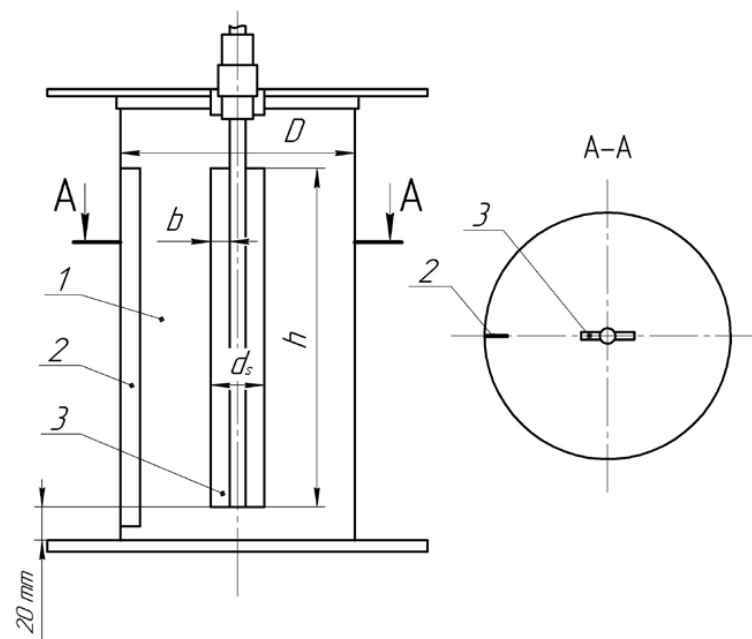


Figure 2. Diagram of the experimental apparatus with a paddle stirrer: 1—body; 2—removable partition; 3—stirrer paddle.

The diameter of the tank body varied from 0.28 to 0.6 m, and its height was 0.3–1.5 m. The paddle stirrer diameter was 0.03–0.12 m, the paddle width was 0.015–0.06 m, the paddle height was 0.05–1.30 m, the removable partition width was 0.02 m, and their number varied from 1 to 3 pieces. A 2.2 kW three-phase motor was used to rotate the stirrer. A US-made ESV402N04TXB LENZE frequency converter was used to change the rotational speed. The voltage and current were measured by a Russian-made non-contact ammeter VAR-M01-083 UHL4, «Meander». The value of the gas content in the liquid layer was determined volumetrically according to the following formula [3]:

$$\varphi = \frac{H_{g-l} - H_L}{H_{g-l}}, \quad (6)$$

where H_L is the height of the liquid layer in the apparatus (m), and H_{g-l} is the height of the gas–liquid layer (m).

The angular velocity of the gas–liquid mixture rotating in the apparatus was determined by supplying a dyestuff and tracking its movement by video filming, followed by data processing [45].

The average surface diameter of the gas bubbles was determined by photographic technique and further calculation [45,46]:

$$d_b = \sqrt{\frac{\sum(N_{bi} \cdot d_{bi}^2)}{\sum N_i}}, \quad (7)$$

where N_i is the number of a certain size of bubbles (pcs), and d_{bi} is the bubble diameter (m). The phase interface was determined as follows [10]:

$$a = \frac{6 \cdot \varphi}{d_b}, \quad (8)$$

where φ is the gas content (-).

Water and a glycerin–water mixture were used as the working media. The temperature of the studied liquids varied from 14 to 60 °C.

Mass transfer at each stage was studied in the context of oxygen absorption from air by water.

The mass transfer intensity was determined based on the model of ideal mixing in a periodic reactor [43]:

$$\frac{dc}{d\tau} = \beta \cdot (c^* - c), \quad (9)$$

where c is the oxygen concentration in the liquid (kg/m^3), c^* is the steady-state oxygen concentration in the liquid (kg/m^3), and β is the mass transfer coefficient (s^{-1}).

The dependence for calculating the mass transfer coefficient from (9) after integration has the form:

$$\beta = \ln[|c^* - c|/A]/T, \quad (10)$$

where coefficient A is determined at $c = c_0$, $T = 0$, c_0 is the initial oxygen concentration in the liquid (kg/m^3), and T is the time (s).

Energy dissipation was calculated according to the formula:

$$\varepsilon = \frac{E}{m}, \quad (11)$$

where E is the internal energy of the gas (W), and m is the liquid mass (kg).

Euler's criterion for stirring power was determined as follows [3]:

$$K_N = \frac{N}{\rho_{mix} \cdot n^3 \cdot d_s^5}, \quad (12)$$

where K_N is the power criterion, N is the stirring power (W), ρ_{mix} is the density of gas–liquid mixture (kg/m^3), n is the rotational speed (s^{-1}), and d_s is the stirrer diameter (m).

The density of the gas–liquid mixture was calculated as follows [3]:

$$\rho_{mix} = \rho_L \cdot (1 - \varphi) + \rho_g \cdot \varphi, \quad (13)$$

where ρ_L is the liquid density (kg/m^3), φ is the gas content, and ρ_g is the density of air (kg/m^3).

Reynolds number was determined as follows:

$$Re = \frac{n \cdot d_s^2 \cdot \rho_{mix}}{\mu}, \quad (14)$$

where n is the rotational speed (s^{-1}), d_s is the stirrer diameter (m), ρ_{mix} is the density of gas–liquid mixture (kg/m^3), and μ is the medium dynamic viscosity coefficient ($\text{Pa} \cdot \text{s}$).

The stirring power was determined on the basis of both the measured current and voltage values and the no-load power.

Numerical simulation was performed in OpenFOAM, which uses a generalized version of the Navier–Stokes equations. The following tank parameters were taken: $D = 0.3$ m, $H_L/D = 1$, $d_s = 0.064$ m, and $b = 0.025$ m, and the liquid used is water.

Before the hydrodynamic analysis of the stirrer, its solid model along with a detailed drawing of its geometric features was prepared. After that, the prepared geometry was subdivided into elements of a computational grid, and the test for grid convergence revealed a computational grid consisting of 600,000 elements of various shapes.

To simulate a rotating flow, the sliding-grid approach was applied, which is best suited for simulating flows in several moving systems of reference [47]. During the simulation, a transient SimpleDyMFoam non-stationary solver was used, which, based on the calculation results, allowed studying the varying rotational speed and pressure values.

In the simulation, a medium with physical and chemical properties corresponding to full-scale tests was set as the working medium. For the computation, the turbulent $k-\epsilon$ model commonly used in computational practice was selected.

3. Results and Discussion

3.1. Gas–Liquid Dispersion Conditions

As the experimental studies showed, to achieve intensive gas–liquid dispersion, the gas vortex cavity has to extend along the stirrer paddle, and the side edges of the paddles must be immersed into the liquid (see Figure 1e). In this case, the rotational speed of the stirrer should be sufficient to generate the required pressure in the local liquid regions behind the paddles. Under these conditions, when the liquid was completely squeezed out from the paddle surface, no intensive gas dispersion was observed.

The depth of the gas vortex cavity and its parameters depend on the angular velocity of the liquid, the rotational speed of the designed stirrer parameters, and the stirrer immersion depth [4,12]. Our studies showed that for a 1.5 m high tank and a stirrer paddle height of 1.3 m, the gas vortex cavity reached the tank bottom when only one partition was installed and the rotational speed was 1200 rpm.

The gas vortex cavity was maintained on the paddle surface by changing the movement of the liquid and its angular velocity by installing one to three partitions on the tank body wall.

Figure 3 shows the changes in the angular velocity of the liquid depending on the rotational speed of the stirrer and the number of partitions.

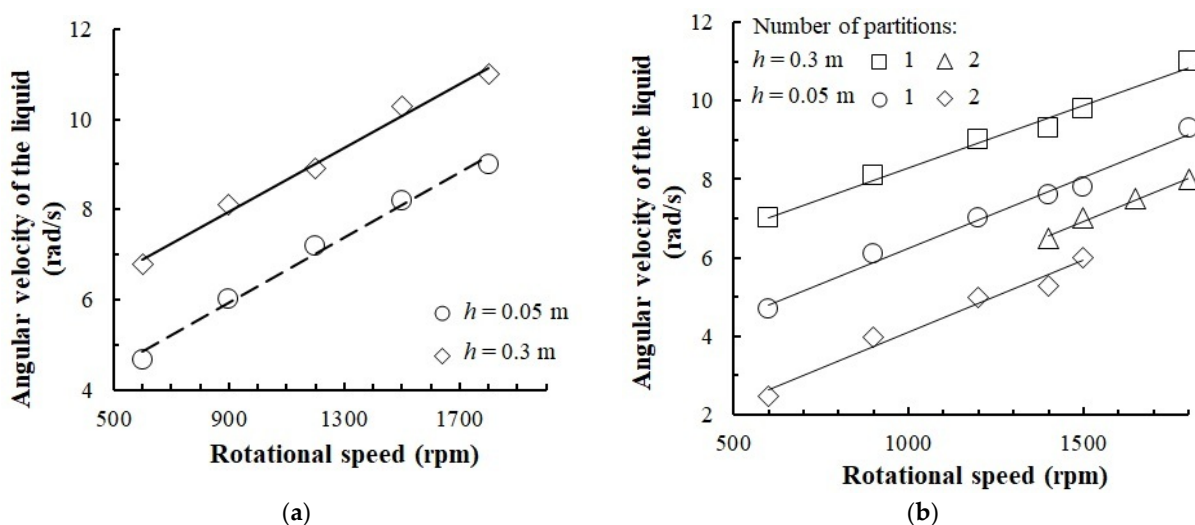


Figure 3. Change in the angular velocity of the gas–liquid medium at a rotational speed of $H_L/D = 1.2$, $D = 0.28$ (m) apparatus without partitions (a) and apparatus with partitions (b) for a different paddle height h .

According to the data presented in Figure 3a, when installing a paddle with a height of $h = 0.3$ m, the angular velocity of the liquid in the tank with no partitions increased by 1.5 times versus a paddle with a height of $h = 0.05$ m.

Installing partitions inside the tank body leads to a decrease in the angular velocity of the liquid (see Figure 3b), which allows, by changing their number, controlling the dimensions of the gas vortex cavity and maintaining the liquid on the paddle surfaces.

The hydrodynamic mode in which intensive gas dispersion began was accompanied by a characteristic sound that was generated when the stirrer speed reached 600–1100 rpm, depending on the number of partitions and the stirrer dimensions.

Figure 4 shows photographs of the vortex and the gas–liquid medium in the tank at different rotational speeds of the stirrer for paddle height $h = 0.3$ m at position (I) and $h = 0.05$ m at position (II). According to the data, at a stirrer rotational speed of 600 rpm, no intensive gas–liquid dispersion was observed (see Figure 4a), either on the paddle $h = 0.3$ m (I) or on the paddle $h = 0.05$ m (II).

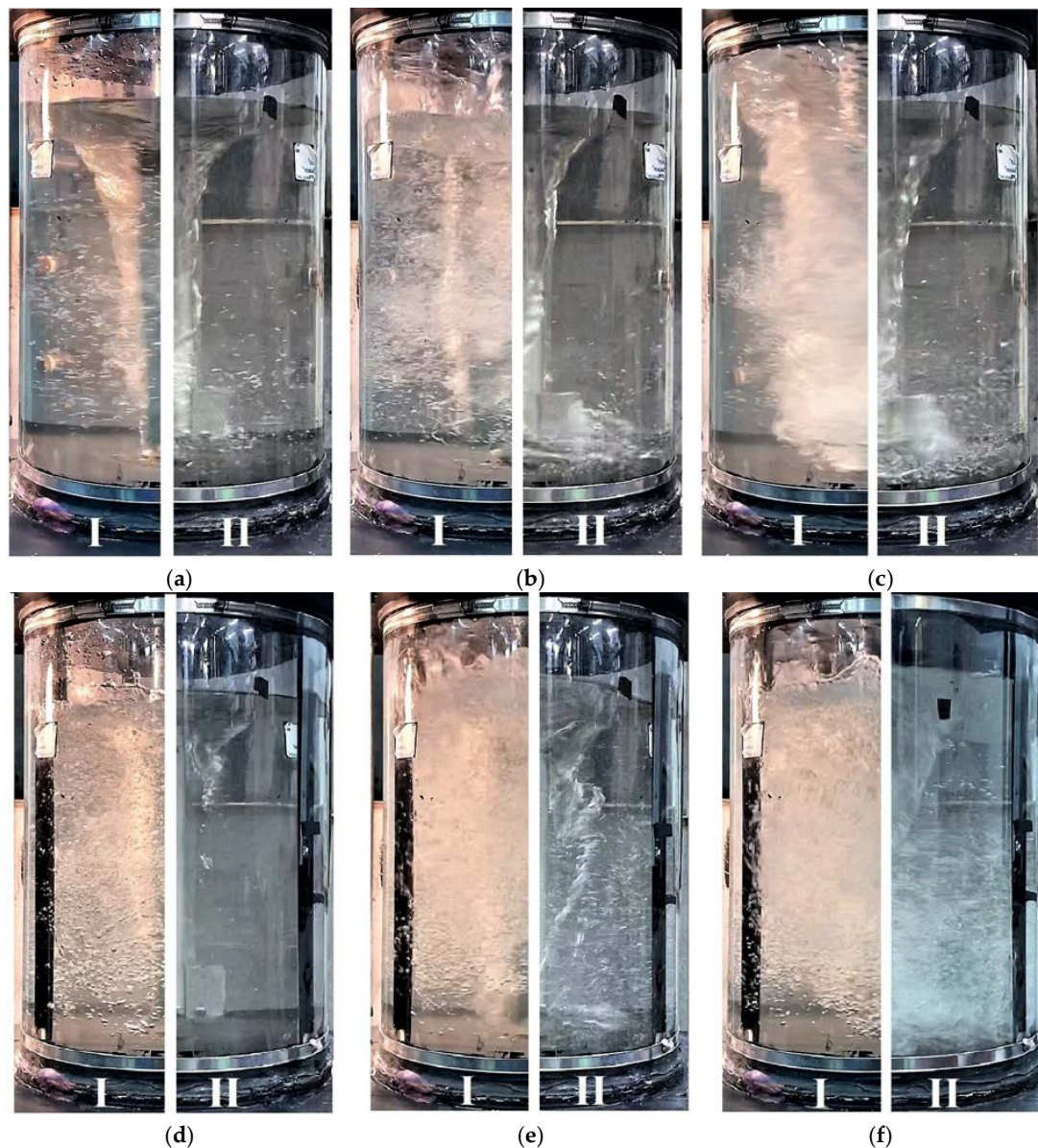


Figure 4. View of the gas–liquid medium in the apparatus without partitions (a–c) and with two partitions (d–f) with a change in the rotational speed at $H_L/D = 1.2$, $D = 0.28$ (m), $d_s = 0.064$ (m), $b = 0.025$ (m), $h = 0.3$ (m) (I), and $h = 0.05$ (m) (II): (a,d) 600 (rpm); (b,e) 900 (rpm); (c,f) 1200 (rpm).

With an increase in the stirrer rotational speed in the tank without partitions, the vortex diameter at the stirrer location becomes commensurate with the width of the stirrer paddle (see Figure 4b,c), and the liquid is squeezed out from the paddle surfaces, which does not provide conditions for intensive gas dispersion and its ejection into the liquid working volume.

Placing at least one partition inside the tank body leads to a decrease in the angular velocity of the liquid, the immersion of the side edges of paddles, and gas dispersion from the stirrer paddle throughout the liquid column height inside the tank (see Figure 4e,f).

A numerical simulation was carried out to determine the pressure drop in the local liquid regions behind the stirrer paddles.

3.2. Simulation Results

Figure 5 presents the calculated values of the pressure of the liquid inside the stirred tank. As established, a reduced pressure was observed behind the stirrer paddles, which confirms the assumption made about the driving force ensuring intensive gas dispersion.

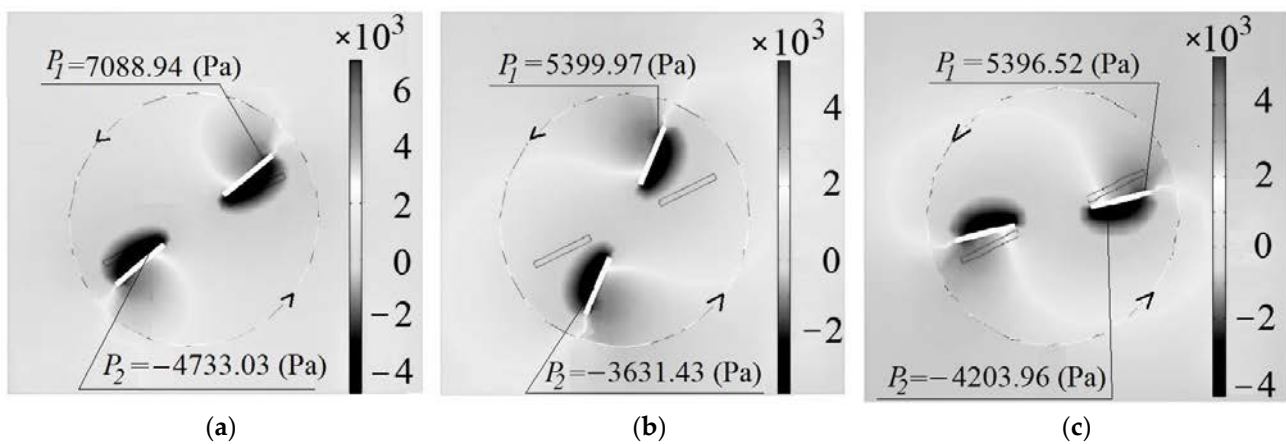


Figure 5. Calculation pressure in fluid behind the stirrer paddles for rotational speed $n = 1000$ (rpm) and paddle height $h = 0.05$ (m) at the calculation time T (s): (a) 1, (b) 4, (c) 6.

Figure 6 shows the changes in the maximum and minimum pressure of the liquid located in the paddle movement region depending on the calculation time and the stirrer rotational speed.

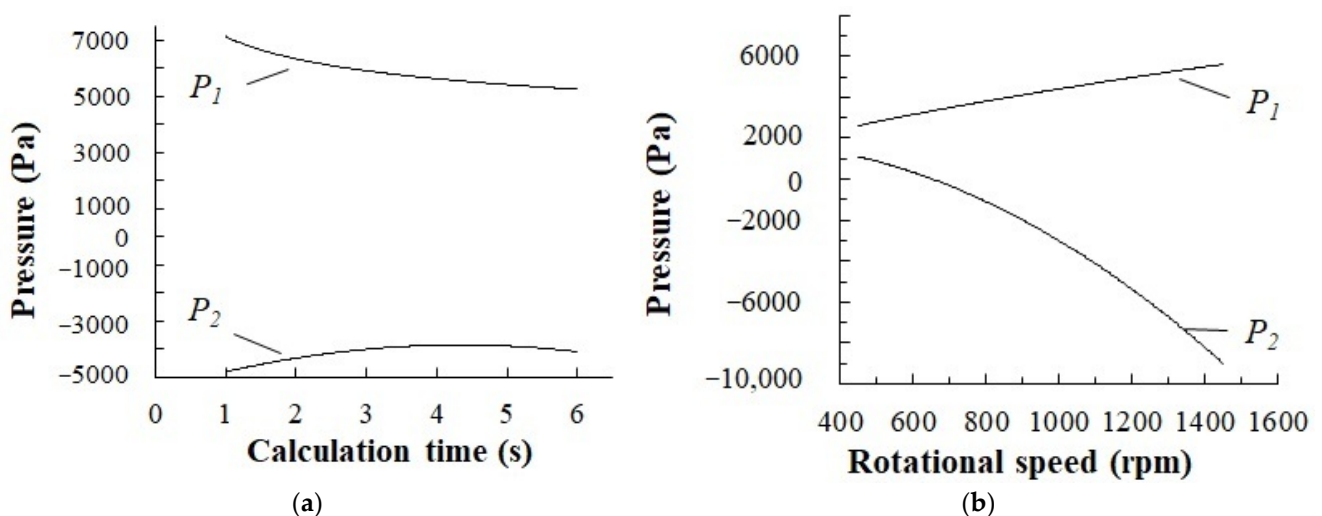


Figure 6. Changes in the maximum (P_1) and minimum (P_2) pressure in the fluid with time in simulation (a) $n = 1000$ (rpm), $h = 0.05$ (m), and the stirrer rotational speed (b).

According to the data presented in Figure 6b, at a rotational speed over 600 rpm, the local pressure behind the paddles becomes lower than the atmospheric pressure, and it drops with an increase in the stirrer rotational speed.

The stirring process simulation (Figure 7b) demonstrates that the reduced pressure regions occur along the entire paddle height (point 1–3). The paddle height increase causes the local region size increase. This is the process driver that conditions the supply of gas from the vortex cavity into the entire volume of liquid, therefore ensuring the gas content growth.

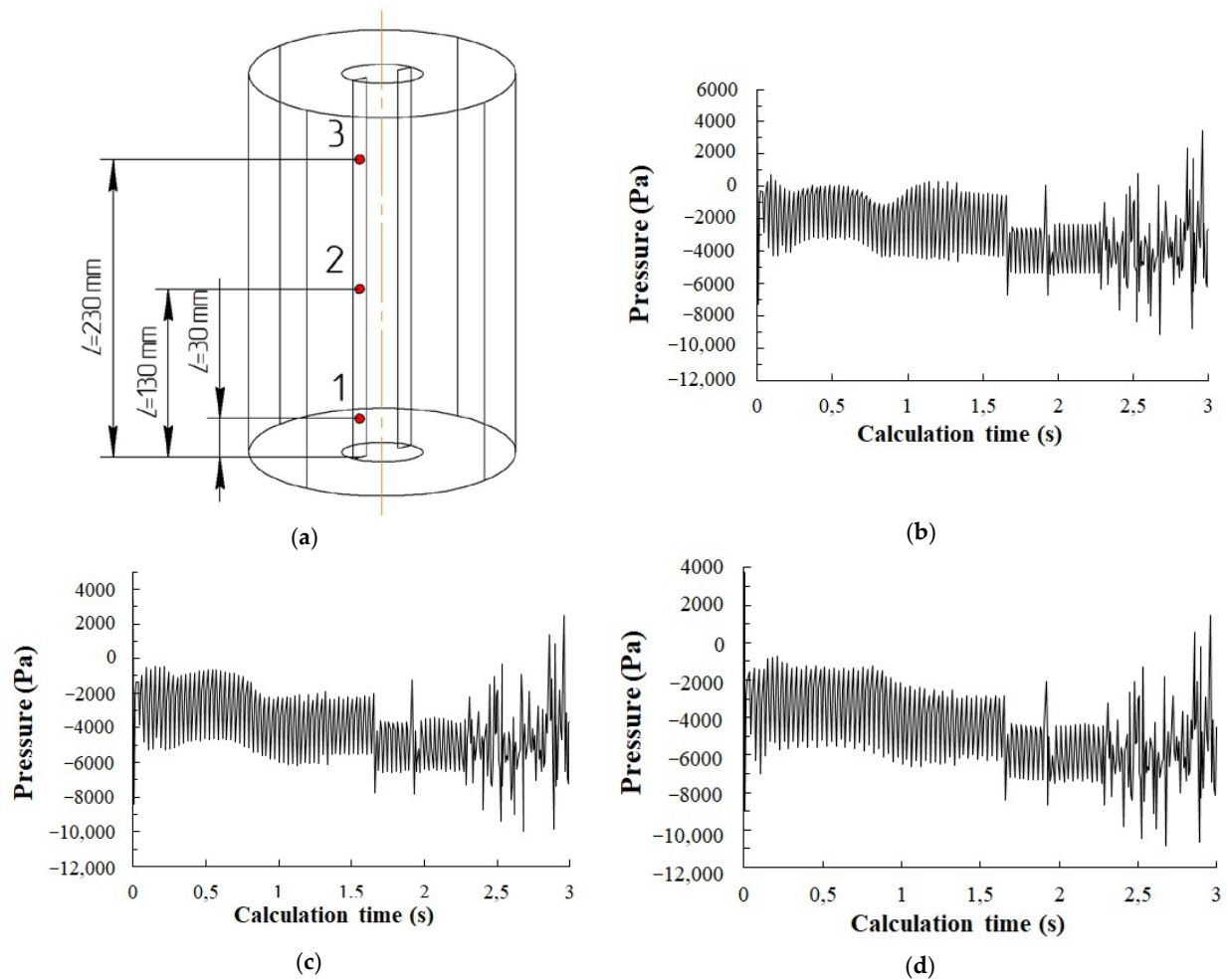


Figure 7. Scheme of a solid model (a) and change in pressure with time (b–d) for a liquid with viscosity $10^{-6}\text{ (m}^2/\text{s)}$, $n = 1000\text{ (rpm)}$, $h = 0.3\text{ (m)}$: (b) $L = 0.3\text{ (m)}$; (c) $L = 0.13\text{ (m)}$; (d) $L = 0.23\text{ (m)}$; (point 1–3) reading points.

Moreover, a numerical simulation was performed to assess the influence made by liquid viscosity on the pressure changes behind the stirrer paddle. The calculation showed that the pressure does not undergo any significant changes within the studied viscosity range (see Figure 8).

Thus, the calculation results demonstrated the presence of regions with reduced liquid pressure behind the stirrer paddles. Subatmospheric pressures were also observed to appear at a stirrer rotational speed of 600 rpm. A change in viscosity over the studied range does not significantly affect the variations in the liquid pressure behind the paddle.

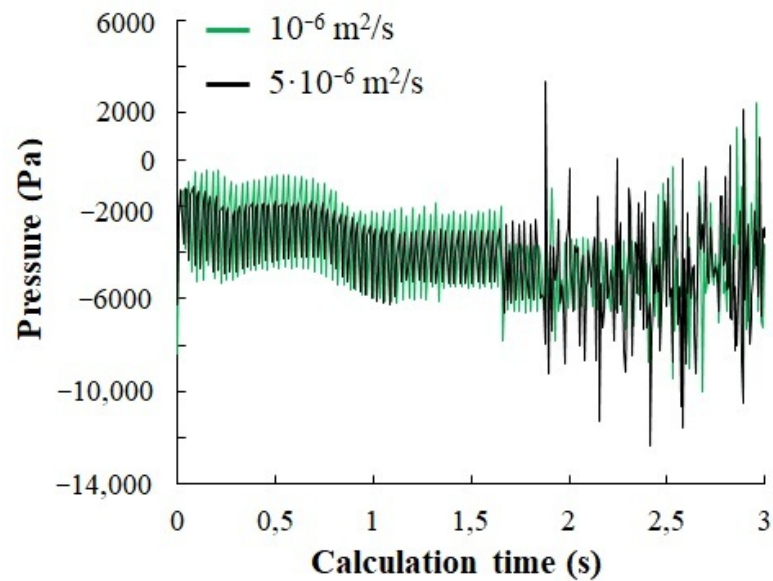


Figure 8. The dependence of pressure on time at different liquid viscosities at $n = 1000$ (rpm), $h = 0.3$ (m), $L = 0.13$ (m).

3.3. Gas Content and Phase Interface

Figures 9 and 10 present the gas content values that we obtained when studying the new gas dispersion method (schematic diagram in Figure 1e) for water and 10% glycerin–water mixture. For a paddle $h = 0.3$ m, the gas content is 2.5 times higher (Figure 9, point 1) compared to a paddle $h = 0.05$ m (Figure 9, point 5).

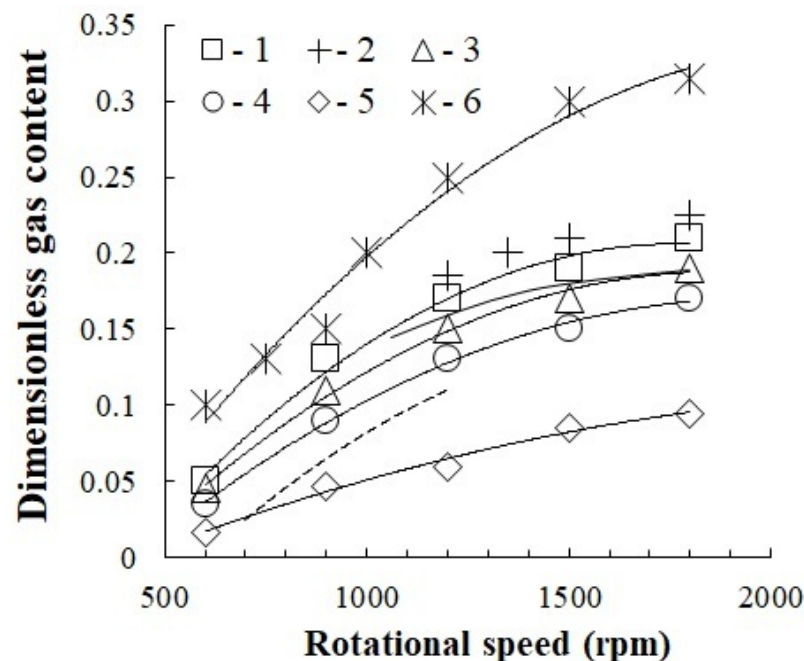


Figure 9. Dependence of gas content on the rotational speed of the stirrer at a water temperature of $23\text{ }^{\circ}\text{C}$, $D = 0.28$ (m), $d_s = 0.064$ (m), $H_L/D = 1.2$, $h = 0.3$ (m). Experimental points (1–6): 1—two partitions; 2—one partition, $H_L/D = 3$; 3—one partition; 4—three partitions; 5—one partition, $h = 0.05$ (m); 6—one partition, 10% glycerin–water. The dotted line is the data from Poncin, S. et al., 2002 [7].

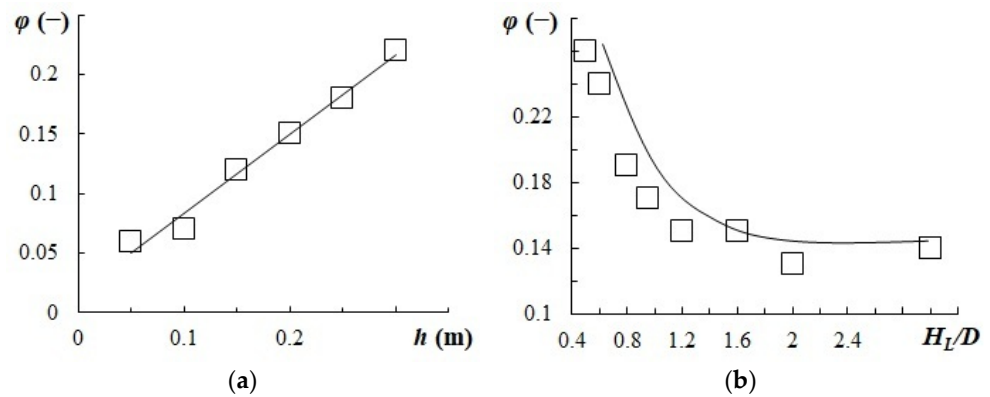


Figure 10. Dependence of gas content on paddle height (a) and the ratio H_L/D (b) at $H_L/D = 1.2$, $D = 0.28$ (m), $n = 1400$ (rpm), $b = 0.025$ (m), $d_s = 0.065$ (m), $h = 0.3$ (m).

An increase in the paddle height leads to an increase in the size of local regions with a reduced liquid pressure behind the paddle along the tank height, which ensures an increase in the gas content.

The proportion of gas in the liquid when the tank was operating on a glycerin–water mixture (Figure 9, point 6) turned out to be higher compared to gas dispersion in the water that comes about as a result of a decrease in surface tension.

According to experimental data shown in Figure 10, the gas content increases with increasing paddle height and decreases with increasing geometric similarity simplex H_L/D .

The established dependence (see Figure 10a) of gas content and the height of the stirrer paddle can also serve as confirmation of the assumption made about the presence of regions with reduced liquid pressure throughout the paddle height.

The average surface diameter of gas bubbles at a water temperature of 20 °C in the tank operating according to the dispersion schematic diagram in Figure 1e was 1.0–1.4 mm, and the phase interface, according to points 7–9 in Figure 11, reached 1000 m^{-1} .

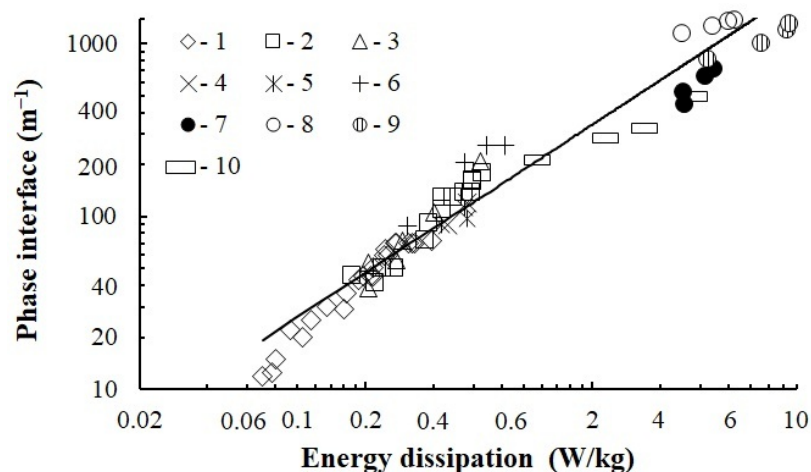


Figure 11. Dependence of the interfacial surface on energy dissipation. Experimental points for bubbling without a stirrer according to [48] (1–6): $D = 0.2$ – 0.5 (m), $H_L/D = 0.8$ – 1.2 ; data of the authors when the apparatus was operated according to the intensive dispersion scheme (Figure 1e) at $D = 0.3$ (m), $H_L/D = 1.2$, $d_s = 0.064$ (m) (7–9): 7— $h = 0.05$ (m); 8— $h = 0.3$ (m), one partition; 9— $h = 0.3$ (m), three partitions; 10—[49] in an apparatus with a turbine stirrer and bubbler.

Based on the photo processing, the dispersive composition of the bubbles in the size interval of 0.2–5 mm and their normal distributions were determined. The maximum number of bubbles under the considered water temperature of 25 °C varies within their diameter interval of 1.0–2.0 mm depending on speed. The angular rotation velocity of the

stirrer increases and the interfacial tension of liquid decreases, causing the decrease in the mean surface diameter of the gas bubble.

3.4. Stirring Power

In this regard, the power values that we obtained (see Figure 12) when studying the tank gas dispersion method, according to the schematic diagram in Figure 1e, are not summarized in terms of the Re number, since the stirring power is greatly influenced by the gas content, which varies both from the liquid temperature and from the stirrer rotational speed.

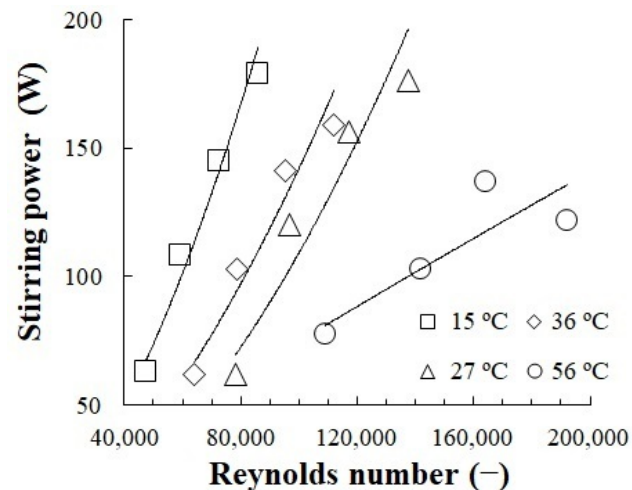


Figure 12. The dependence of the mixing power on the Reynolds number at $h = 0.3$ (m), one partition, $H_L/D = 1.2$, $d_s = 0.064$ (m), $D = 0.28$ (m) at $n = 600$ – 2400 (rpm).

Figure 13a presents the changes in the power from the stirrer rotational speed and the number of partitions in the tank. In the presence of one or two partitions, the N values do not differ significantly (Figure 13a, points 1 and 2), which apparently is due to the gas content effect. However, a further increase in the number of partitions leads to an increase in power (Figure 13a, point 3).

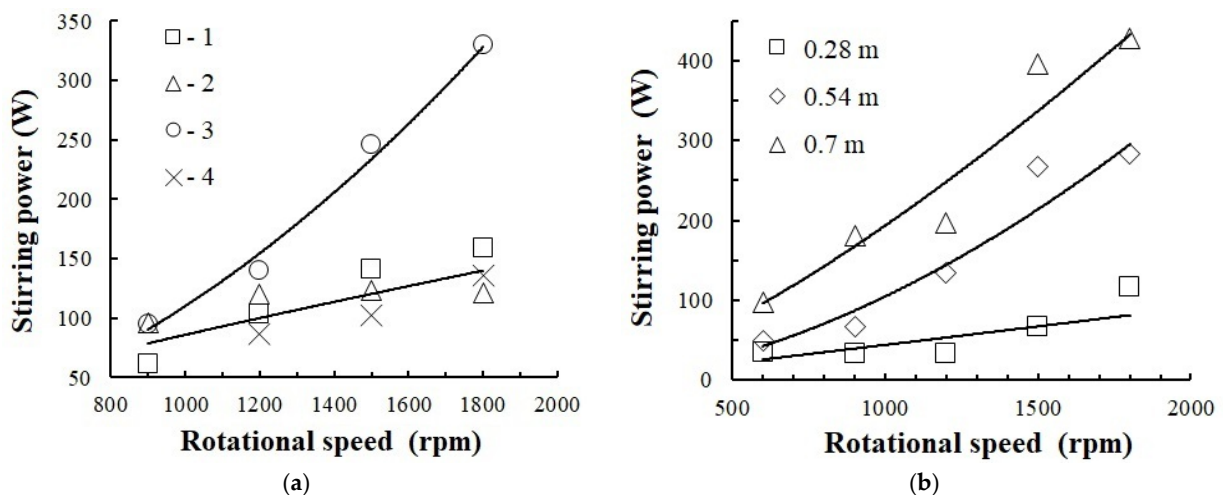


Figure 13. Dependence of the mixing power on the rotational speed: (a) $H_L/D = 1.2$, $D = 0.280$ (m), $d_s = 0.064$ (m) with variation in the number of partitions: 1—one partition, $h = 0.3$ (m); 2—two partitions, $h = 0.3$ (m); 3—three partitions, $h = 0.3$ (m); 4—one partition, $h = 0.05$ (m); (b) $D = 0.280$ (m), one partition, $d_s = 0.075$ (m), $h = H_L$ with varying liquid column height H_L .

An increase in the liquid column height inside the tank leads to an increase in the stirring power (Figure 13b, points 1–3).

Figures 14 and 15 present the values of the power criterion calculated taking into account the gas content according to Formula (12).

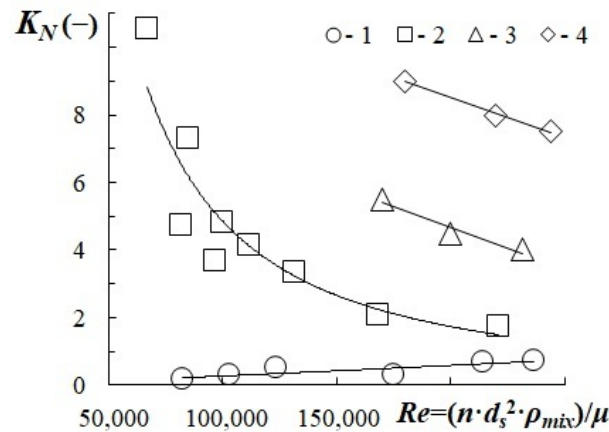


Figure 14. Dependence of the power criterion on the Reynolds number for the stirrer $h = 0.05$ (m), at a temperature of 13–60 °C, $n = 600$ –2400 (rpm), $H_L/D = 1.2$, $d_s = 0.064$ (m) with a variation in the number of partitions: 1—without partition; 2—one partition; 3—two partitions; 4—three partitions.

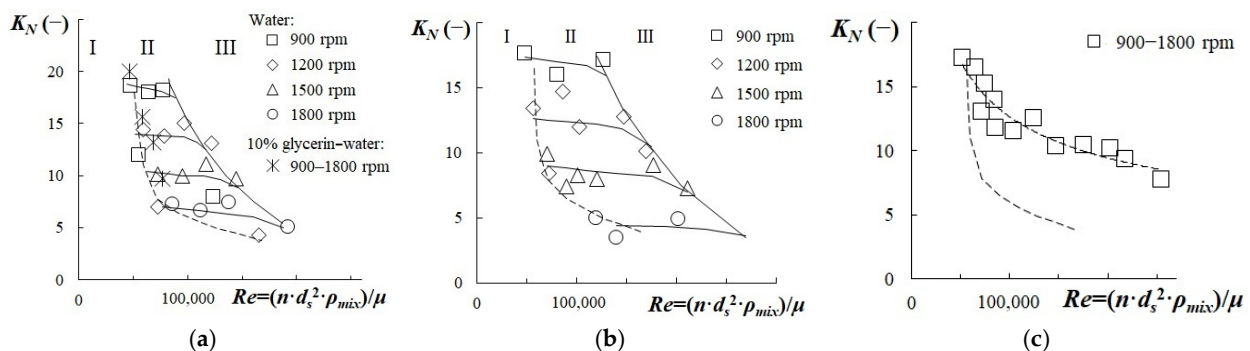


Figure 15. Dependence of the power criterion on the Reynolds number at $H_L/D = 1.2$, $D = 0.28$ (m), water temperature 13–60 °C, for different rotational speed: (a) one partition; for water (b) two partitions and (c) three partitions, $H_L = 0.3$ (m); the dotted line is the apparatus without partitions; (I) turbulent operating conditions, (II) bubble operating conditions and the region of developed turbulent interaction (III).

For a paddle $h = 0.05$ m, the value of the power criterion (Figure 14, point 1) during liquid stirring in the tank without partitions was $K_N = 0.7$, which data from numerous studies [12] confirm. The slight increase in the power criterion at high Reynolds numbers in the studied case is due to an increase in the gas content.

When a paddle $h = 0.3$ m is installed in the tank without partitions, the power criterion increases (Figure 15, dashed line) in comparison with a short paddle.

Figure 15 presents the values of the power criterion in the presence of partitions in the tank wall for the paddle $h = 0.3$ m. Three areas of influence of the Reynolds number on K_N can be distinguished: turbulent operating conditions (I), where the viscous friction forces predominate; bubble operating conditions (II), where the power loss is significantly affected by the gas content; and the region of developed turbulent interaction (III).

In the bubble operating region, the power criterion weakly depends on the Reynolds number, which is also observed in self-priming stirred tanks [6] (Figure 15a, point 6). It can also be noted that with increasing gas content, the value of K_N decreases. In the case of three partitions (see Figure 16c) the bubble effect is absent.

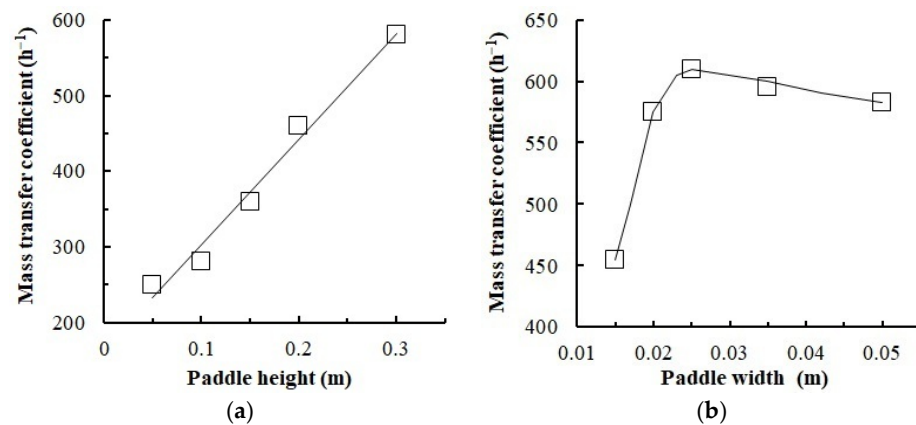


Figure 16. The dependence of the mass transfer coefficient on the height (a) and width of the paddle (b) at $H_L/D = 1.2$, $n = 1400$ (rpm), $D = 0.28$ (m), one partition.

Thus, to generate gas–liquid dispersion in the tank according to the schematic diagram presented in Figure 1d, reducing the stirring power requires the minimum number of partitions to be installed inside the tank. In the region of intensive dispersion at 1200–2400 rpm and gas content 0.15–0.2, the power criterion calculated taking into account the gas content was $K_N = 4$ –5.

3.5. Mass Transfer Experiments

Figures 16 and 17 present experimental data on the mass transfer in the studied gas dispersion method according to the schematic diagram in Figure 1e. The value of the mass transfer coefficient increases with an increase in the stirrer paddle length (Figure 16a) due to a higher gas content. The mass transfer intensity increases with an increase in the stirrer paddle width and at a certain level remains practically unchanged (Figure 16b).

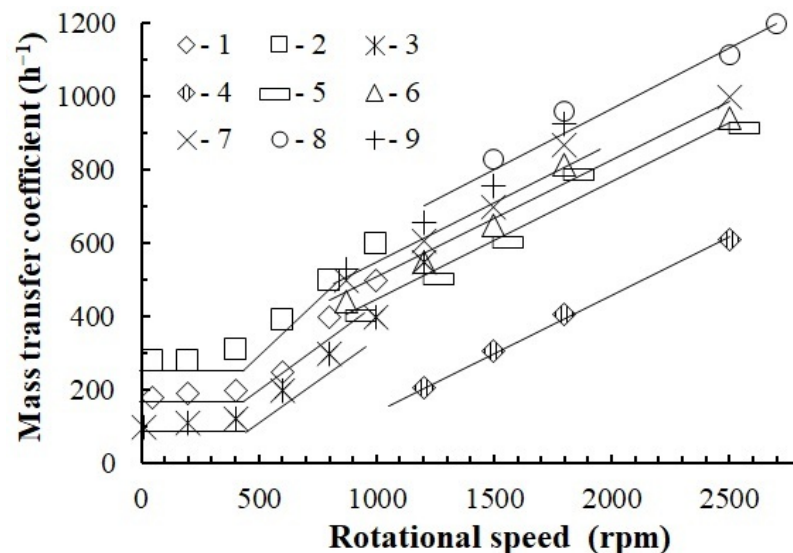


Figure 17. Mass transfer coefficient as a function of rotational speed of the stirrer. Experimental points (1–3) according to [49] stirrer with bubbler at $D = 0.375$ (m), $H_L/D = 1$, $d_s = 0.11$ (m): 1— $u_g = 0.018$ (m/s); 2— $u_g = 0.03$ (m/s); 3— $u_g = 0.04$ (m/s); experimental points (4–9) data of the authors on the intensive dispersion method at $H_L/D = 1.2$, $D = 0.28$ (m), $d_s = 0.070$ (m): 4—one partition, $h = 0.05$ (m); 5—one partition, $h = 0.3$ (m); 6—two partitions, $h = 0.3$ (m); 7—three partitions, $h = 0.3$ (m); 8—one partition, $h = 0.3$ (m), four paddles; 9—one partition, $h = 0.3$ (m), $H_L/D = 3$.

Increasing the number of paddles from two to four allowed for increasing the mass transfer coefficient by 1.4 times (Figure 17, point 8).

Figure 18 shows the dependence of the mass transfer coefficient on energy dissipation.

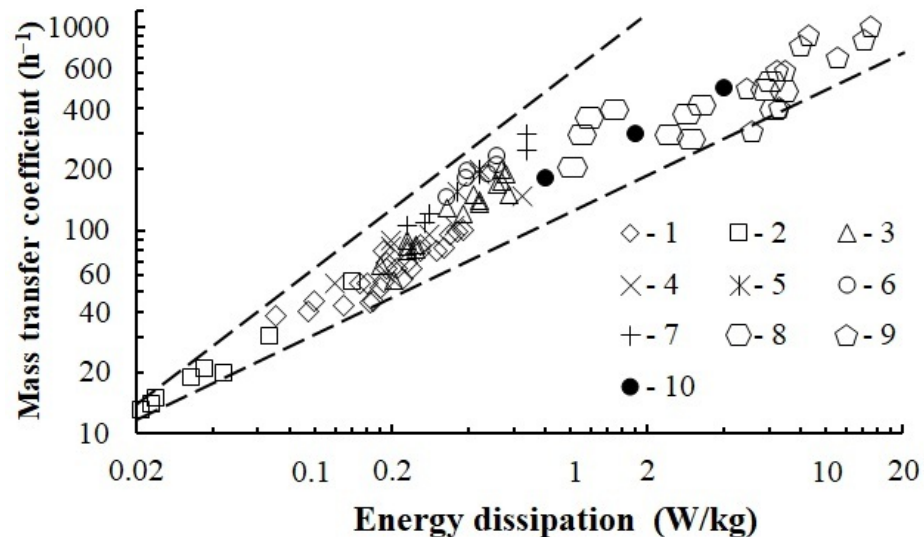


Figure 18. Dependence of the mass transfer coefficient on energy dissipation. Experimental points (1–7) bubbling without a stirrer [48]; 8—stirrer with bubbler (Figure 1a), [49] at $D = 0.375$ (m), $H_L/D = 1$, $d_s = 0.110$ (m), $u_g = 0.018$ – 0.04 (m/s); 9—the method under study (Figure 1e) at $H_L/D = 1.2$, $D = 0.280$ (m); 10—data [7].

Figure 19 shows the dependence of the mass transfer coefficient on the energy dissipation and phase interface according to the data in Figure 18.

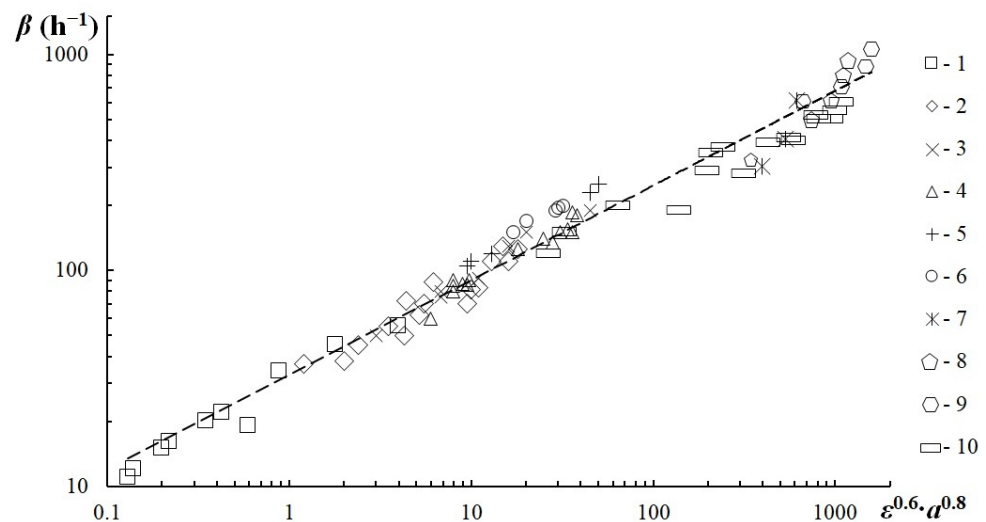


Figure 19. Change in the mass transfer coefficient from the parameter $\varepsilon^{0.6} \cdot a^{0.8}$. Experimental points (1–6) according to [48] during bubbling; (7–9) data of the studied method according to the intensive dispersion scheme (Figure 1e): 7— $H_L = 0.05$ (m); 8— $H_L = 0.3$ (m), 1 partition; 9— $H_L = 0.3$ (m), 3 partitions; 10—data [49] apparatus with a stirrer.

Data processing allowed obtaining the following equation for the mass transfer coefficient:

$$\beta = 30 \cdot \left[\varepsilon^{0.6} \cdot a^{0.8} \right]^{0.45}, \quad (15)$$

where β is the mass transfer coefficient (h^{-1}), ε is the energy dissipation (W/kg), and a is the phase interface (m^{-1}).

The dependence summarizes the data obtained both during bubbling and in the stirred tank.

The surface mass transfer coefficient with intensive dispersion reached $0.3 \cdot 10^{-3} \text{ m/s}$.

4. Conclusions

1. A new method of gas dispersion from an open vortex cavity in a stirrer apparatus was developed to intensify the mass exchange without additional mechanical gas feeding to simplify the general stirrer structure and increase the liquid layer height. The dispersion method can efficiently be used to develop high-performance bioreactors, chemical reactors, aerotanks, and floatation plants. Used in various units, this method allows modifying the mass transfer coefficient and gas content across a broad range of values.
2. The presence of reduced pressure regions in liquid behind the rotating stirrer paddle has been experimentally found and confirmed through the numerical simulation method. Intensive gas dispersion has been discovered to occur as the pressure drop between the liquid region behind the paddle and the vortex gas cavity exceeds 1000 Pa. A condition for the intensive dispersion of gas from the vortex cavity into the reduced pressure region is the need to keep the gas cavity open in the stirrer location, to keep the liquid on the paddle surface and to maintain the stirrer rotation velocity of 600 rpm or more.
3. The gas content value, gas bubble diameter, and phase surface were determined from the experiment. An increase in the paddle height was shown to lead to higher gas content and energy dissipation.
4. With the presented method, gas–liquid dispersion allows developing the phase separation border to 1000 m^{-1} and the mass exchange coefficient to 1200 h^{-1} without mechanical gas feeding into the apparatus.
5. The dependency of the stirrer power criterion on Reynolds number was determined. An increase in the gas content was proven to lead to a decrease in the KN value. At rotation speeds of 1200–2400 rpm and a gas content of 0.15–0.2, the power criterion calculated by factoring in the gas content value in the intensive dispersion region equals to $K_N = 4\text{--}5$.
6. The study demonstrates that with the intensive gas dispersion method, the mass transfer coefficient values are comparable with those calculated for the apparatus with a turbine stirrer with a gas supply of 7–20 m^3/h . In this case, energy dissipation of the rotating stirrer reaches 25 W/kg .
7. The dependency for calculating the mass transfer coefficient inside the apparatus with the dispersion method developed was made to factor in energy dissipation and phase surface in further calculations.

Author Contributions: N.A.V. came up with the conceptual framework and designed the experiments. A.S.F. performed numerical simulation of the experiments. A.V.B. performed the majority of the experiments and D.A.Z. performed additional experiments. O.P.Z. generalization of the obtained data. All authors contributed to the data analysis and the writing of this paper. All authors have read and agreed to the published version of the manuscript.

Funding: The work described in the paper «Method for Intensive Gas–Liquid Dispersion in a Stirred Tank» was supported by the Ministry of Science and Higher Education of the Russian Federation within the framework of the State Assignment of the Technology and Equipment for the Chemical Processing of Biomass of Plant Raw Materials Project FEFE-2020 0016.

Data Availability Statement: This article contains all the data generated or evaluated throughout the research.

Acknowledgments: This work was carried out using the equipment of the Krasnoyarsk Regional Center for Collective Use of the Krasnoyarsk Research Centre of the KSC SB RAS. We would like to thank the staff of the Collaborative Use Centre for their assistance in the research.

Conflicts of Interest: The authors declare no conflict of interest.

Abbreviations

A	coefficient
a	interphase surface (m^{-1})
b	width paddle (m)
c	oxygen concentration in the liquid (kg/m^3)
D	body shell diameter (m)
D_l	oxygen diffusion coefficient in water (m^2/s)
d	diameter (m)
E	internal energy of gas (W)
H	height (m)
h	height paddle (m)
K_N	dimensionless power criterion
L	readout altitude (m)
m	liquid mass (kg)
N	stirring power (W)
n	rotational speed (rpm)
N_i	number of a certain size of bubbles (pcs)
P	pressure (Pa)
Q	liquid flow rate (m^3/s)
Re	Reynolds number
Sc	Schmidt criterion
Sh	Sherwood criterion
s	stirrer pitch (m)
T	time (s)
u	velocity (m/s)
V	volume of liquid (m^3)
β	mass transfer coefficient (h^{-1})
ϵ	energy dissipation (W/kg)
μ	medium dynamic viscosity coefficient (Pa·s)
ν	kinematic viscosity of the fluid (m^2/s)
ρ	density (kg/m^3)
σ	surface tension coefficient (N/m)
φ	dimensionless gas content

Indices

*	steady-state
b	bubble
g	gas
$g-l$	gas-liquid
L	liquid
mix	mixture
s	stirrer
0	initial
1	maximum
2	minimum

References

- Scargiali, F.; Busciglio, A.; Grisafi, F.; Brucato, A. Oxygen transfer performance of unbaffled stirred vessels in view of their use as biochemical reactors for animal cell growth. *Chem. Eng. Trans.* **2012**, *27*, 205–210.
- Tsao, G.T.N. Vortex behavior in the waldhof fermentor. *Biotechnol. Bioeng.* **1968**, *10*, 177–188. [[CrossRef](#)]
- Sokolov, V.N.; Yablokova, M.A. *Microbiological Industry Equipment*; Mashinostroenie: Leningrad, Russia, 1988; 278p.

4. Rao, A.; Kumar, B.; Patel, A. Vortex behavior in an unbaffled surface aerator. *Sci. Asia* **2009**, *35*, 183–188. [[CrossRef](#)]
5. Guan, X.; Li, X.; Yang, N.; Liu, M. CFD simulation of gas-liquid flow in stirred tanks: Effect of drag models. *Chem. Eng. J.* **2020**, *386*, 121554. [[CrossRef](#)]
6. Scargiali, F.; Busciglio, A.; Grisafi, F.; Brucato, A. Gas-liquid-solid operation of a high aspect ratio self-ingesting reactor. *Int. J. Chem. React. Eng.* **2012**, *10*, 839–845. [[CrossRef](#)]
7. Poncin, S.; Nguyen, C.; Midoux, N.; Breyse, J. Hydrodynamics and volumetric gas-liquid mass transfer coefficient of a stirred vessel equipped with a gas-inducing impeller. *Chem. Eng. Sci.* **2002**, *57*, 3299–3306. [[CrossRef](#)]
8. Saravanan, K.; Mundale, V.D.; Joshi, J.B. Gas Inducing Type Mechanically Agitated Contactors. *Ind. Eng. Chem. Res.* **1994**, *33*, 2226–2241. [[CrossRef](#)]
9. Newell, R.; Grano, S. Hydrodynamics and scale up in Rushton turbine flotation cells: Part 2. Flotation scale-up for laboratory and pilot cells. *Int. J. Miner. Process.* **2006**, *81*, 65–78. [[CrossRef](#)]
10. Sokolov, V.N.; Domansky, I.V. *Gas-Liquid Reactors*; Mashinostroenie: Leningrad, Russia, 1976; 216p.
11. Busciglio, A.; Caputo, G.; Scargiali, F. Free-surface shape in unbaffled stirred vessels: Experimental study via digital image analysis. *Chem. Eng. Sci.* **2013**, *104*, 868–880. [[CrossRef](#)]
12. Deshpande, S.S.; Kar, K.K.; Walker, J.; Pressler, J.; Su, W. An experimental and computational investigation of vortex formation in an unbaffled stirred tank. *Chem. Eng. Sci.* **2017**, *168*, 495–506. [[CrossRef](#)]
13. Ciofalo, M.; Brucato, A.; Grisafi, F.; Torracca, N. Turbulent flow in closed and free-surface unbaffled tanks stirred by radial impellers. *Chem. Eng. Sci.* **1996**, *51*, 3557–3573. [[CrossRef](#)]
14. Rielly, C.D.; Evans, G.M.; Davidson, J.F.; Carpenter, K.J. Effect of vessel scale up on the hydrodynamics of a self-aerating concave blade impeller. *Chem. Eng. Sci.* **1992**, *47*, 3395–3402. [[CrossRef](#)]
15. Hsu, Y.C.; Chen, T.Y.; Chen, J.H.; Lay, C.W. Ozone Transfer into Water in a Gas-Inducing Reactor. *Ind. Eng. Chem. Res.* **2002**, *41*, 120–127. [[CrossRef](#)]
16. Conway, K.; Kyle, A.; Rielly, C. Gas-liquid-solid operation of a vortex-ingesting stirred tank reactor. *Chem. Eng. Res. Des.* **2002**, *80*, 839–845. [[CrossRef](#)]
17. Hsu, Y.C.; Huang, C.J. Characteristics of a new gas-induced reactor. *AIChE J.* **1996**, *42*, 3146–3152. [[CrossRef](#)]
18. Joshi, J.B.; Sharma, M.M. Mass transfer and hydrodynamic characteristics of gas inducing type of agitated contactors. *Can. J. Chem. Eng.* **1977**, *55*, 683–695. [[CrossRef](#)]
19. Forrester, S.E.; Rielly, C.D. Modelling the increased gas capacity of self-inducing impellers. *Chem. Eng. Sci.* **1994**, *49*, 5709–5718. [[CrossRef](#)]
20. Heim, A.; Krasa-wski, A.; Ryzski, E.; Stelmach, J. Aeration of bioreactors by self-aspirating impellers. *Chem. Eng. J. Biochem. Eng. J.* **1995**, *58*, 59–63. [[CrossRef](#)]
21. Hultholm, S.E.; Lilya, L.; Nyman, B. Stirring Apparatus and Method of Gas Mixing in a Closed Reactor. EAPO Patent EA003815B1, 6 June 2003. Available online: <https://www.eapo.org/ru/publications/publicat/viewpubl.php?id=003815> (accessed on 3 February 2023).
22. Greenshields, C.J. *OpenFOAM The Open Source CFD Toolbox: User Guide*; OpenFOAM Foundation Ltd.: London, UK, 2022; 237p. Available online: <http://foam.sourceforge.net/docs/Guides-a4/OpenFOAMUserGuide-A4.pdf> (accessed on 3 February 2023).
23. Chen, G.; Xiong, Q.; Morris, P.J.; Paterson, E.G.; Sergeev, A.; Wang, Y.-C. OpenFOAM for Computational Fluid Dynamics. *Not. AMS* **2014**, *61*, 354–363. [[CrossRef](#)]
24. Li, L.; Gu, Z.; Xu, W.; Tan, Y.; Fan, X.; Tan, D. Mixing mass transfer mechanism and dynamic control of gas-liquid-solid multiphase flow based on VOF-DEM coupling. *Energy* **2023**, *272*, 127015. [[CrossRef](#)]
25. Voinov, N.A.; Frolov, A.S.; Zemtsov, D.A. Method for Saturation of Liquid with Gas in Apparatus with a Mixer. Paten RU 2790167 C1, 14 February 2023. Available online: <https://patenton.ru/patent/RU2790167C1> (accessed on 15 February 2023).
26. Adamiak, R.; Karcz, J. Effects of Type and Number of Impellers and Liquid Viscosity on the Power Characteristics of Mechanically Agitated Gas-Liquid Systems. *Chem. Pap.* **2007**, *61*, 16–23. [[CrossRef](#)]
27. Cudak, M. Hydrodynamic Characteristics of Mechanically Agitated Air-Aqueous Sucrose Solutions. *Chem. Process Eng.* **2014**, *35*, 97–107. [[CrossRef](#)]
28. Hassan, I.T.M.; Robinson, C.W. Stirred-Tank Mechanical Power Requirement and Gas Holdup in Aerated Aqueous Phases. *AIChE J.* **1977**, *23*, 48–56. [[CrossRef](#)]
29. Lee, B.W.; Dudukovic, M.P. Determination of flow regime and gas holdup in gas-liquid stirred tanks. *Chem. Eng. Sci.* **2014**, *109*, 264–275. [[CrossRef](#)]
30. Alves, S.S.; Maia, C.I.; Vasconcelos, J.M.T. Experimental and modelling study of gas dispersion in a double turbine stirred tank. *Chem. Eng. Sci.* **2002**, *57*, 487–496. [[CrossRef](#)]
31. Leshev, I.; Peev, G. Film flow on a horizontal rotating disk. *Chem. Eng. Process. Process Intensif.* **2003**, *42*, 925–929. [[CrossRef](#)]
32. Fasano, J.B.; Myers, K.J.; Janz, E.E. Effect of geometric variations on the performance of gas dispersion impellers with semicircular blades. *Can. J. Chem. Eng.* **2011**, *89*, 961–968. [[CrossRef](#)]
33. Garcia-Ochoa, F.; Gomez, E. Theoretical prediction of gas-liquid mass transfer coefficient, specific area and hold-up in sparged stirred tanks. *Chem. Eng. Sci.* **2004**, *59*, 2489–2501. [[CrossRef](#)]
34. Karcz, J.; Siciarz, R.; Bielka, I. Gas hold-up in a reactor with dual system of impellers. *Chem. Pap.* **2004**, *58*, 404–409. Available online: <http://fez.schk.sk/view/changeme:5192> (accessed on 4 February 2023).

35. Kerdouss, F.; Bannari, A.; Proulx, P. CFD modeling of gas dispersion and bubble size in a double turbine stirred tank. *Chem. Eng. Sci.* **2006**, *61*, 3313–3322. [[CrossRef](#)]
36. Bates, R.L.; Fondy, P.L.; Corpstein, R.R. Examination of Some Geometric Parameters of Impeller Power. *Ind. Eng. Chem. Process Des. Dev.* **1963**, *2*, 310–314. [[CrossRef](#)]
37. Furukawa, H.; Kato, Y.; Inoue, Y.; Kato, T.; Tada, Y.; Hashimoto, S. Correlation of Power Consumption for Several Kinds of Mixing Impellers. *Int. J. Chem. Eng.* **2012**, *2012*, 106496. [[CrossRef](#)]
38. Khabibrakhmanov, R.B.; Mukhachev, S.G. Power and mass transfer characteristics of a bioreactor with perforated disc stirrers. *Proc. Univ. Appl. Biochem. Biotechnol.* **2019**, *9*, 737–749. [[CrossRef](#)]
39. Scargiali, F.; Busciglio, A.; Grisafi, F.; Brucato, A. Simplified dynamic pressure method for measurement in aerated bioreactors. *Biochem. Eng. J.* **2010**, *49*, 165–172. [[CrossRef](#)]
40. Scargiali, F.; Russo, R.; Grisafi, F.; Brucato, A. Mass transfer and hydrodynamic characteristics of a high aspect ratio self-ingesting reactor for gas–liquid operations. *Chem. Eng. Sci.* **2007**, *62*, 1376–1387. [[CrossRef](#)]
41. Osipov, A.V.; Bogatykh, S.A. *On the Optimization of Geometric Reactors with a Circulation Loop*; Mashinostroenie: Leningrad, Russia, 1972; pp. 103–108.
42. Dyakonov, S.G.; Elizarov, V.I.; Laptev, A.G. Model of mass transfer in the bubbling layer of a contact device based on the concept of an active (inlet) section. *Theor. Found. Chem. Eng.* **1991**, *25*, 783–795.
43. Ramm, V.M. *Gas Absorption*; Khimiya: Moscow, Russia, 1976; 656p.
44. Litmans, B.A.; Kukurechenko, I.S.; Tumanov, Y.V. Investigation of mass transfer in the liquid phase in a bubbling apparatus with mechanical agitation at high energy inputs. *Theor. Found. Chem. Eng.* **1974**, *8*, 344–350.
45. Voinov, N.A.; Zhukova, O.P.; Nikolaev, N.A. Hydrodynamics of the Vortex Stage with Tangential Swirlers. *Theor. Found. Chem. Eng.* **2010**, *44*, 213–219. [[CrossRef](#)]
46. Shahbazi, B.; Rezai, B.; Chehreh Chelgani, S.; Koleini, S.M.J.; Noaparast, M. Estimation of diameter and surface area flux of bubbles based on operational gas dispersion parameters by using regression and ANFIS. *Int. J. Min. Sci. Technol.* **2013**, *23*, 343–348. [[CrossRef](#)]
47. Jasak, H. Dynamic Mesh Handling in OpenFOAM. In Proceedings of the 47th AIAA Aerospace Sciences Meeting Including The New Horizons Forum and Aerospace Exposition, Orlando, FL, USA, 5–8 January 2009. [[CrossRef](#)]
48. Voinov, N.A.; Frolov, A.S.; Bogatkova, A.V.; Zemtsov, D.A.; Zhukova, O.P. Hydrodynamics and mass transfer at the vortex stage and during bubbling. *Theor. Found. Chem. Eng.* **2019**, *6*, 972–983. [[CrossRef](#)]
49. Voinov, N.A.; Gurulev, K.V.; Volova, T.G. Mass exchange in a bioreactor with a mixer during cultivation of hydrogen-oxidizing bacteria *Ralstonia eutropha* in a mode of polyhydroxyalkanoate synthesis. *Biotechnol. Russ.* **2005**, *3*, 98–107.

Disclaimer/Publisher’s Note: The statements, opinions and data contained in all publications are solely those of the individual author(s) and contributor(s) and not of MDPI and/or the editor(s). MDPI and/or the editor(s) disclaim responsibility for any injury to people or property resulting from any ideas, methods, instructions or products referred to in the content.